Nanoscale Res Lett (2010) 5:603–607
DOI 10.1007/s11671-009-9513-5

NANO EXPRESS

Synthesis and Photocatalytic Activity of Anatase TiO_2 Nanoparticles-coated Carbon Nanotubes

Yi Xie · Sung Hwan Heo · Seung Hwa Yoo · Ghafar Ali · Sung Oh Cho

Received: 17 November 2009 / Accepted: 10 December 2009 / Published online: 24 December 2009

Abstract A simple and straightforward approach to prepare TiO_2-coated carbon nanotubes (CNTs) is presented. Anatase TiO_2 nanoparticles (NPs) with the average size ~8 nm were coated on CNTs from peroxo titanic acid (PTA) precursor even at low temperature of 100 °C. We demonstrate the effects of CNTs/TiO_2 molar ratio on the adsorption capability and photocatalytic efficiency under UV–visible irradiation. The samples showed not only good optical absorption in visible range, but also great adsorption capacity for methyl orange (MO) dye molecules. These properties facilitated the great enhancement of photocatalytic activity of TiO_2 NPs-coated CNTs photocatalysts. The TiO_2 NPs-coated CNTs exhibited 2.45 times higher photocatalytic activity for MO degradation than that of pure TiO_2.

Keywords TiO_2 · Carbon nanotubes · Nanoparticles · Photocatalyst · Methyl orange

Introduction

TiO_2 has been one of the most widely investigated and used materials over the past decades [1–3], because it is nontoxic, easy to be made, inexpensive and chemically stable. In recent years, TiO_2-based nanomaterials have attracted significant research attention due to their broad applications in the fields of water and air purification [4, 5], H_2 production [6, 7], and photovoltaic and photoelectrochemical cells [8, 9].

Y. Xie · S. H. Heo · S. H. Yoo · G. Ali · S. O. Cho (✉)
Department of Nuclear and Quantum Engineering, Korea Advanced Institute of Science and Technology (KAIST), 373-1 Guseong, Yuseong, Daejeon 305-701, Republic of Korea
e-mail: socho@kaist.ac.kr

However, one of the major factors that limit the efficiency of TiO_2 photocatalysis is its fast recombination of photo-generated electron/hole pairs, which releases energy in the form of unproductive heat or photons. To solve this problem, many efforts have been made to reduce charge recombination and enhance photocatalytic activity of TiO_2 [10]. Recently, synthesis of TiO_2-CNTs composites has also attracted significant attention to increase the photocatalytic efficiency of TiO_2 [11–21]. Synthetic methods of TiO_2-CNTs composites include sol–gel [16], chemical vapor deposition (CVD) [18, 19], hydrothermal deposition [20], electrospinning technique [21], etc. Most of the composite materials exhibited better photocatalytic performances than pure TiO_2 because they provide a large surface area and prevent charge recombination by trapping photo-excited electrons generated from TiO_2. Furthermore, due to the conducting properties of CNTs, electrons that are transferred from TiO_2 to CNTs could move freely along CNTs and thus the oxidative reactivity is enhanced. For example, CNTs coated with TiO_2 exhibit higher photodegradation efficiency for phenol [22] and better photocatalytic inactivation of bacterial endospores [23] than CNTs or TiO_2 alone.

However, most of the synthetic approaches of CNTs-TiO_2 composites require special or expensive devices [18, 21], or high temperature process [19, 24]. Herein, we present a very simple and straightforward wet chemical process to synthesize composites comprising anatase TiO_2 NPs-coated CNTs, which can be prepared at low temperature of 100 °C. By varying the ratio of TiO_2/CNTs, a series of composites were prepared in order to optimize the synthetic condition of the TiO_2 NPs-coated CNTs composites that exhibit the best photocatalytic activity. The photocatalytic property of the products was evaluated by degradation of MO under UV–visible irradiation.

Experimental

Synthesis of TiO_2 NPs-coated CNTs

A simple strategy was designed for the preparation of TiO_2 NPs-coated CNTs, using peroxo titanic acid (PTA) as precursor of TiO_2. PTA solution was prepared using the same chemical route as reported elsewhere [25]. The reagents CNTs, titanium tetrachloride ($TiCl_4$), and ammonia solution were purchased from Hanwha Nanotech Corp., Sigma–Aldrich, and Junsei chemical, respectively. The process could be schematically displayed in Scheme 1. Briefly, CNTs was mixed with PTA solution under strong magnetic stirring and ultrasonic dispersion (Scheme 1a). The mixture was then heated at 100 °C for 24 h in a temperature-controlled oil bath equipped with a magnetic stirrer and a reflux condenser. During the heat treatment, PTA adsorbed on CNTs surface could be transformed to anatase TiO_2 (Scheme 1b). Finally, the resulted dark precipitates were filtered and dried at 60 °C for 24 h to obtain the TiO_2 NPs-coated CNTs nanocomposites (Scheme 1c). For the comparison, pure TiO_2 NPs were also prepared using the same wet chemical process without an addition of CNTs.

Characterization

The crystal structure of the samples was investigated by using powder X-ray diffraction (XRD) and Raman spectra. XRD was performed with Cu Kα radiation on a D/MAX-RB X-ray diffractometer (Rigaku, Japan), and Raman analysis was performed on a LabRAM HR instrument (Horiba Jobin–Yvon, France) in air environment. The morphologies and size of the samples were investigated using a Tecnai G2 F30 field emission transmission electron microscope (FETEM, FEI). UV–visible diffuse reflectance spectra (UV–Vis DRS) were performed on a S4100 UV–Vis spectrophotometer.

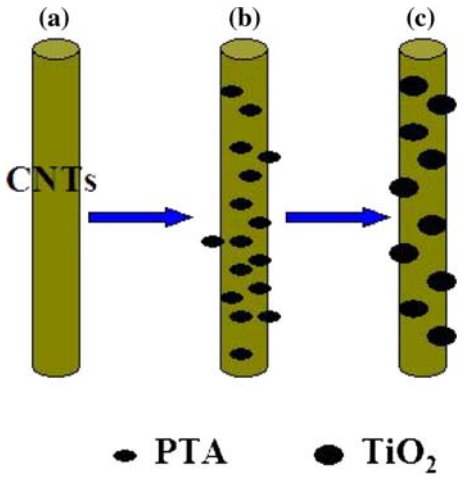

Scheme 1 Schematic illustration of the formation process of TiO_2 NPs-coated CNTs

Photocatalytic Activity Measurements

Photocatalytic decomposition of MO was examined by optical absorption spectroscopy. Typically, 10 mg of photocatalyst was put into 40.0 mL of MO aqueous solution (10 mg/L) in a 50-mL beaker. Prior to irradiation, the mixture was ultrasonicated in a water bath for 2 min to ensure good dispersion of the photocatalysts. Subsequently, the mixture was stirred in darkness for 20 min in order to establish adsorption/desorption equilibrium between MO molecules and the surface of the photocatalysts. The mixture was then illuminated with a 500-W Xe lamp under a magnetic stirring. The solution of 2.0 mL was drawn out, and the MO solution was separated from the photocatalysts by centrifugation to determine the concentration of MO using a S4100 UV–Vis spectrophotometer.

Results and Discussion

Photocatalyst Characterization

TEM images of the as-synthesized samples are shown in Fig. 1. The selected area electron diffraction (SAED) pattern (Fig. 1a, inset) shows polycrystalline diffraction rings, which are indexed to (101), (004), (200) and (105) planes of anatase TiO_2. The particle size of the TiO_2 on the surface of CNTs is ~8 nm (Fig. 1c). In addition, the

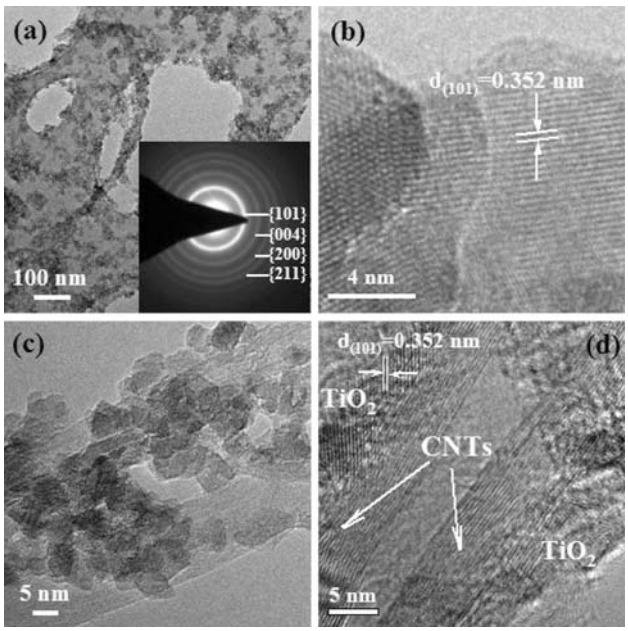

Fig. 1 TEM image of TiO_2 NPs-coated CNTs (**a**), and HRTEM images of pure TiO_2 (**b**) and anatse TiO_2 NPs-coated CNTs (**c**, **d**)

measured lattice distance of 0.35 nm (Fig. 1b, d) is a good agreement with (101) lattice distance of anatase TiO_2. These results indicate that anatase TiO_2 NPs-coated CNTs have been successfully synthesized under low temperature of 100 °C.

It has been reported [26] that six Raman active modes for anatase TiO_2, $A_{1g} + 2B_{1g} + 3E_g$, could be detected at 144 cm^{-1} (E_g), 197 cm^{-1} (E_g), 399 cm^{-1} (B_{1g}), 513 cm^{-1} (A_{1g}), 519 cm^{-1} (B_{1g}), and 639 cm^{-1} (E_g), and the peaks at 250, 450, and 620 cm^{-1} are due to the Ti–O–Ti bond of rutile spectrum. Raman spectra provided by Fig. 2 indicate the presence of anatase TiO_2 for all the samples synthesized with different CNTs/TiO_2 M ratios. The two weak peaks centered at around 1,347 and 1,580 cm^{-1} are due to CNTs [27], which cannot be observed for pure TiO_2 (Fig. 2, inset, below right). In addition, the peak corresponding to the E_{1g} mode of anatase TiO_2 significantly shift from ~148 to 155 cm^{-1} compared with that of pure TiO_2 (Fig. 2, inset, upper left). It has been reported that such a blue shift could be attributed to phonon confinement caused by a decrease in crystal size of anatase [28] or an increased surface strain of TiO_2 caused by the adsorption of surfactants [29]. In our study, the size of TiO_2 NPs is calculated to be around 8 nm, which will be further discussed later. Consequently, the blue shift of Raman peak might be caused by CNTs, which act a similar effect as surfactant. Comparatively, the ratio of peak intensity between TiO_2 and CNTs increases with the decreasing CNTs/TiO_2 molar ratios, which indicates that the concentration of TiO_2 increased within the samples.

Figure 3 displays the XRD pattern of pure TiO_2 and TiO_2 NPs-coated CNTs nanocomposites. As depicted in Fig. 3a, c, the diffraction peaks at $2\theta = 25.2°$, 37.8°, 47.9°, 54.0° and 62.6° match exactly with (101), (004), (200), (105) and (204) reflections of anatase TiO_2 (JCPDS: 21-1272). The characteristic peaks for CNTs at the positions of $2\theta = 25.9°$ and 43.2° are observed for pure CNTs sample (Fig. 3b), which is similar with the results reported elsewhere [30]. However, the peak at $2\theta = 25.9°$ cannot be found clearly in the TiO_2 NPs-coated CNTs except the weak peak at $2\theta = 43.2°$ (Fig. 3c). This is because the main peak of CNTs at $2\theta = 25.9°$ is overlapped by that of anatase TiO_2 at $2\theta = 25.2°$. The peaks of anatase TiO_2 tend to shield those of CNTs, for the crystalline extent of TiO_2 is stronger than that of CNTs. This could be observed from the comparison of XRD peak intensity between pure TiO_2 (Fig. 3a) and pure CNTs (Fig. 3b). In addition, the average crystal diameter of the pure TiO_2 (Fig. 3a) was found to be ~8 nm from the XRD patterns, which was calculated from the largest XRD peak centered at $2\theta = 25.2°$ by the well-known Scherrer's equation.

Figure 4 provides the UV–vis DRS spectra of the synthesized samples. One can observe that pure TiO_2 exhibit band-edge absorptions around 387 nm (Fig. 4a) typically for anatase phase. However, pure CNTs display absorbance over the entire visible light region. Besides the band-edge absorption around 387 nm, additional wide optical absorptions in visible light region are also observed for TiO_2 NPs-coated CNTs. Figure 4 also indicates that the spectral absorbance of the TiO_2 NPs-coated CNTs increased generally with the increasing of CNT content, which might be associated with the absorption of CNTs. This visible light absorbance property can facilitate the enhancement of photocatalytic property of the TiO_2-based nanomaterials.

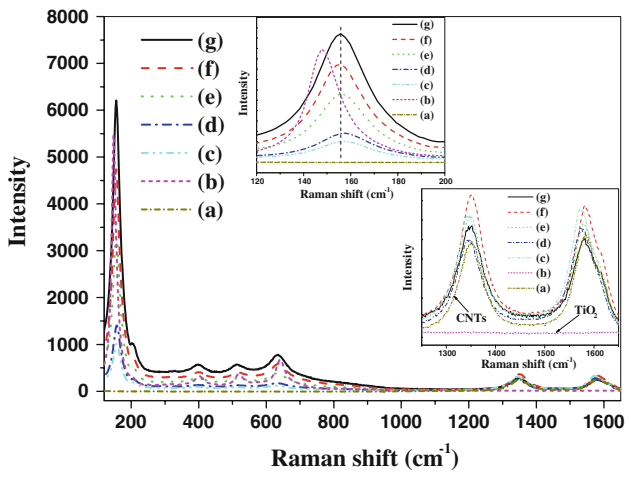

Fig. 2 Raman spectra of pure CNTs (**a**), TiO_2 (**b**), and TiO_2 NPs-coated CNTs synthesized with CNTs/TiO_2 molar ratio of 4/1 (**c**), 2/1 (**d**), 1/1 (**e**), 1/2 (**f**) and 1/4 (**g**)

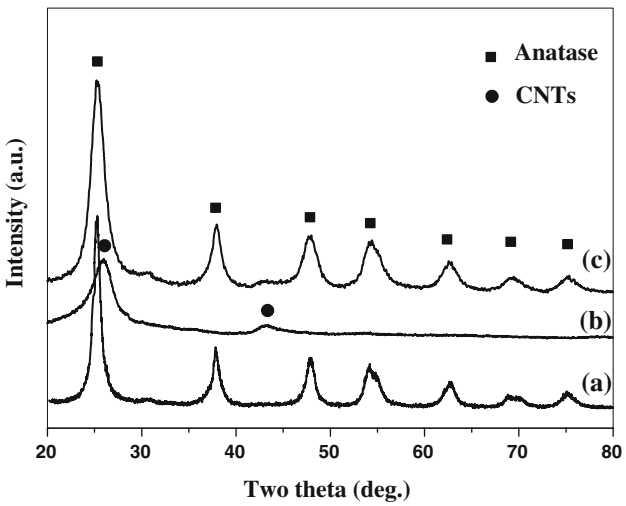

Fig. 3 XRD patterns of pure TiO_2 (**a**), CNTs (**b**) and TiO_2 NPs-coated CNTs (**c**)

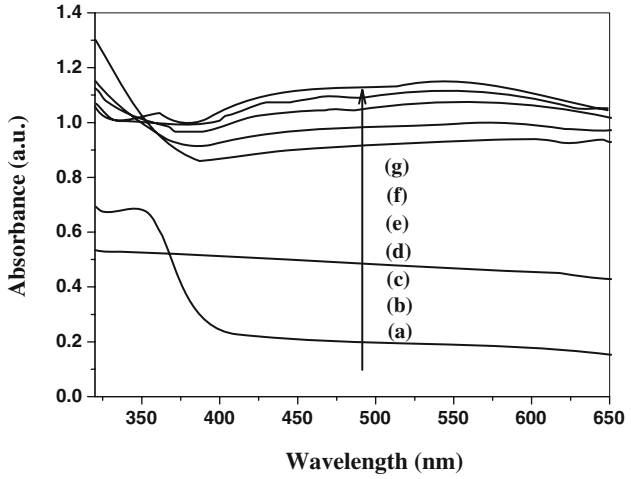

Fig. 4 UV–vis DRS of pure TiO_2 (**a**), CNTs (**b**) and TiO_2 NPs-coated CNTs synthesized with CNTs/TiO_2 molar ratio of 1/4 (**c**), 1/2 (**d**), 1/1 (**e**), 2/1 (**f**), and 4/1 (**g**)

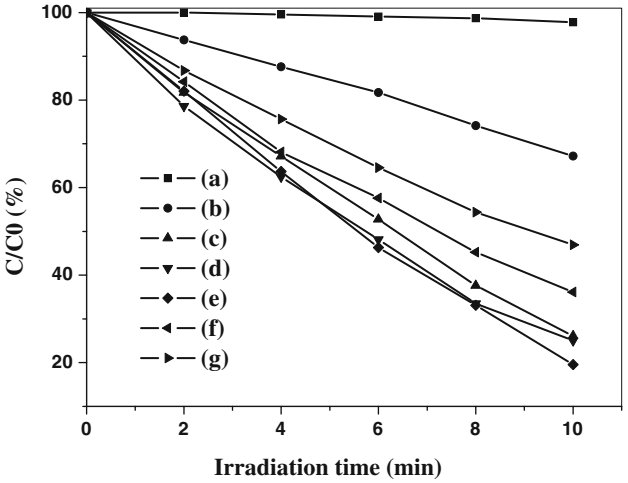

Fig. 5 Photodegradation of MO solutions over CNTs (**a**), TiO_2 (**b**) and TiO_2 NPs-coated CNTs synthesized with CNTs/TiO_2 molar ratio of 1/4 (**c**), 1/2 (**d**), 1/1 (**e**), 2/1 (**f**) and 4/1 (**g**). C0 and C is the initial concentration of MO before irradiation and after irradiation for a period of time, respectively

Photocatalytic Activity of the TiO_2 NPs-coated CNTs

Figure 5 confirms the photodecomposition of dye MO on pure TiO_2 and TiO_2 NPs-coated CNTs photocatalysts. Pure CNTs showed little photocatalytic activity (Fig. 5a), and pure TiO_2 showed only 32.8% photocatalytic decomposition for MO after 10 min of irradiation (Fig. 5b). As can be seen from Fig. 5c–g, the molar ratio of CNTs/TiO_2 affects greatly the photocatalytic activity. Generally the photocatalytic activity increases initially and decreases with increasing the molar ratio of CNTs/TiO_2. Among all of the photocatalysts, the samples prepared with CNTs/TiO_2 molar ratio of 1:1 exhibits the highest photodegradation efficiency with a MO conversion of 80.5% after 10 min of irradiation (Fig. 5e), which is 2.45 times higher than that of pure TiO_2.

It has been widely accepted that photocatalytic properties of TiO_2-based catalysts are governed by various parameters, such as surface area, particle size, and the surface hydroxyl groups. First of all, CNTs provide a large surface area to enhance the adsorption capability for dye molecules. Figure 6 provides the UV–Vis absorption spectra of MO solution over various samples, before (Fig. 6A) and after (Fig. 6B) the irradiation with a Xe lamp. A decrease in the concentration occurred after the samples were dispersed into the MO aqueous solution and subsequently stirred for 20 min in darkness, revealing that parts of the MO molecules were adsorbed on the surface of samples. In addition, the adsorption capability of TiO_2 NPs-coated CNTs was enhanced with increasing the CNT content (Fig. 6A). Especially, pure CNTs exhibited the highest adsorption capacity. This strong adsorption property for dye molecules could affect the photocatalytic activity of TiO_2-based samples. However, excess amount of CNTs would shield TiO_2 from absorbing light and thus weaken the photocatalytic efficiency. Second, it was reported that the relative position of the CNT conduction band edge permit the transfer of electrons from the anatase TiO_2 surface to CNT, allowing charge separation and consequently reducing recombination of photo-excited electron/hole pairs [11]. Last, CNTs facilitate the adsorption of more hydroxyl group on the surface of the TiO_2 NPs-coated CNTs composites [31], which benefit for photocatalysis. All of these properties account for the highest photocatalytic efficiency for TiO_2 NPs-coated CNTs with CNTs/TiO_2 molar ratio of 1:1.

Conclusion

We have demonstrated that composites of anatase TiO_2 NPs-coated CNTs can be straightforwardly prepared by a simple wet chemical method. The molar ratio of CNTs/TiO_2 affects the adsorption capability of the final products, and consequently influences the photocatalytic activity. By optimization, TiO_2 NPs-coated CNTs sample with CNTs/TiO_2 molar ratio of 1:1 exhibits 2.45 times higher efficiency than that of pure TiO_2 NPs. The present chemical method is much simpler than previous-reported methods including CVD and electrospinning technique, and is suitable for large-scale production. Because of the efficient adsorption capability and prominent photodegradation efficiency, the anatase TiO_2 NPs-coated CNTs might be used for other desired applications, such as photovoltaic and photochemical cells, sensor, and hydrogen production.

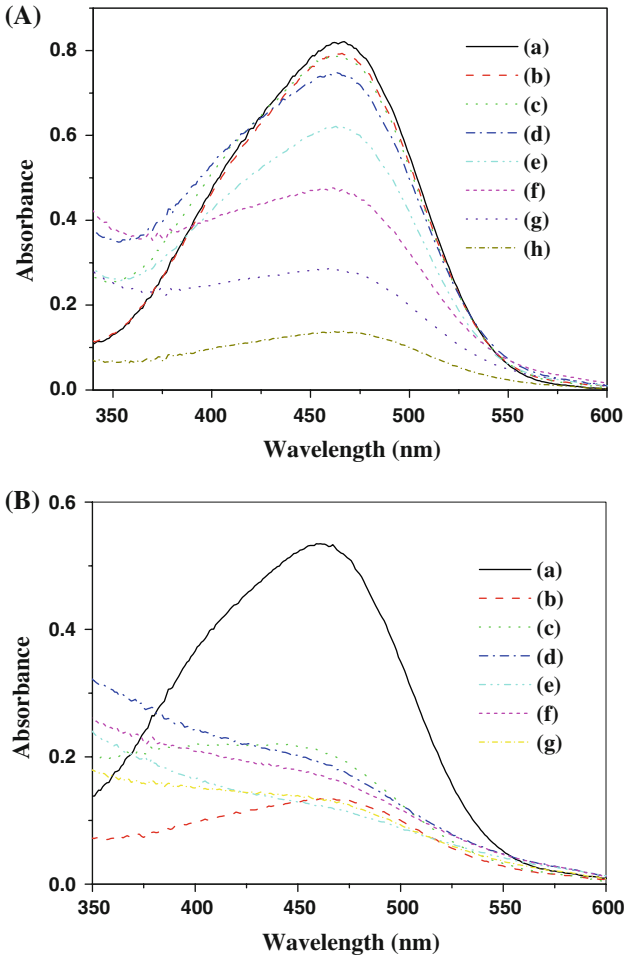

Fig. 6 **A** Absorption spectra of original MO solution of 10 mg/L (*a*) and MO solution before irradiation over various samples: pure TiO_2 (*b*), TiO_2 NPs-coated CNTs with CNTs/TiO_2 molar ratios of 1/4 (*c*), 1/2 (*d*), 1/1 (*e*), 2/1 (*f*), and 4/1 (*g*), and pure CNTs (*h*). **B** Absorption spectra of MO solution after 10 min of irradiation over various samples: pure TiO_2 (*a*), pure CNTs (*b*), and TiO_2 NPs-coated CNTs with CNTs/TiO_2 molar ratios of 1/4 (*c*), 1/2 (*d*), 1/1 (*e*), 2/1 (*f*), and 4/1 (*g*)

Acknowledgments This work was supported by the Korea Science and Engineering Foundation (KOSEF) grant funded by the Korea Ministry of Education, Science and Technology (MEST) (No. 2009-0081819).

References

1. A. Fujishima, K. Honda, Nature **238**, 37 (1972)
2. H.G. Yang, C.C. Sun, S.Z. Qiao, J. Zou, G. Liu, S.C. Smith, H.M. Cheng, G.Q. Lu, Nature **453**, 638 (2008)
3. R. Buonsanti, V. Grillo, E. Carlino, C. Giannini, T. Kipp, R. Cingolani, P.D. Cozzoli, J. Am. Chem. Soc. **130**, 11223 (2008)
4. T. Suprabha, H.G. Roy, J. Thomas, K.P. Kumar, S. Mathew, Nanoscale Res. Lett. **4**, 144 (2009)
5. G. Cappelletti, S. Ardizzone, C.L. Bianchi, S. Gialanella, A. Naldoni, C. Pirola, V. Ragaini, Nanoscale Res. Lett. **4**, 97 (2009)
6. N.G. Petrik, G.A. Kimmel, J. Phys. Chem. C **113**, 4451 (2009)
7. K. Dai, T. Peng, D. Ke, B. Wei, Nanotechnology **20**, 125603 (2009)
8. K.H. Yu, J.H. Chen, Nanoscale Res. Lett. **4**, 1 (2009)
9. M. Law, L.E. Greene, J.C. Johnson, R. Saykally, P.D. Yang, Nat. Mater. **4**, 455 (2005)
10. C.M. Wang, A. Heller, H. Gerischer, J. Am. Chem. Soc. **114**, 5230 (1992)
11. Y. Yao, G. Li, S. Ciston, R.M. Lueptow, K.A. Gray, Environ. Sci. Technol. **42**, 4952 (2008)
12. B. Liu, H.C. Zeng, Chem. Mater. **20**, 2711 (2008)
13. C.S. Kuo, Y.H. Tseng, H.Y. Lin, C.H. Huang, C.Y. Shen, Y.Y. Li, S.I. Shah, C.P. Huang, Nanotechnology **18**, 465607 (2007)
14. D. Eder, A.H. Windle, Adv. Mater. **20**, 1787 (2008)
15. H.Q. Song, X.P. Qiu, F.S. Li, W.T. Zhu, L.Q. Chen, Electrochem. Commun. **9**, 1416 (2007)
16. B. Gao, G.Z. Chen, G.L. Puma, Appl. Catal. B-Environ. **89**, 503 (2009)
17. L.C. Chen, Y.C. Ho, W.S. Guo, C.M. Huang, T.C. Pan, Electrochim. Acta **54**, 3884 (2009)
18. H.T. Yu, X. Quan, S. Chen, H.M. Zhao, Y.B. Zhang, J. Photochem. Photobiol. A Chem. **200**, 301 (2008)
19. S. Orlanducci, V. Sessa, M.L. Terranova, G.A. Battiston, S. Battiston, R. Gerbasi, Carbon **44**, 2839 (2006)
20. T. Sainsbury, D. Fitzmauriceand, Chem. Mater. **16**, 3780 (2004)
21. K. Shahar, S. Judith, P. Yaron, C. Yachin, Langmuir **21**, 5600 (2005)
22. W. Wang, P. Serp, P. Kalck, J.L. Faria, Appl. Catal. B **56**, 305 (2005)
23. S.H. Lee, S. Pumprueg, B. Moudgil, W. Sigmund, Colloids Surf. B **40**, 93 (2005)
24. Y.D. Yang, L.T. Qu, L.M. Dai, T.-S. Kang, M. Durstock, Adv. Mater. **19**, 1239 (2007)
25. Y. Xie, Q.N. Zhao, X.J. Zhao, Y.Z. Li, Catal. Lett. **118**, 231 (2007)
26. M. Mikami, S. Arakanura, O. Kitao, H. Arakwa, Phys. Rev. B **66**, 155213 (2002)
27. S. Wang, L.J. Ji, B. Wu, Q.M. Gong, Y.F. Zhu, J. Liang, Appl. Surf. Sci. **255**, 3263 (2008)
28. D. Bersani, P.P. Lottici, X.-Z. Ding, Appl. Phys. Lett. **72**, 73 (1998)
29. C.Y. Xu, P.X. Zhang, L. Yan, J. Raman Spectrosc. **32**, 862 (2001)
30. S.W. Lee, W.M. Sigmund, Chem. Commun. **6**, 780 (2003)
31. Y. Yu, J.C. Yu, J.G. Yu, Y.C. Kwok, Y.K. Che, J.C. Zhao, L. Ding, W.K. Ge, P.K. Wong, Appl. Catal. A Gen. **289**, 186 (2005)